Two-dimensional Thermal Diffusion Equation Solver Based on Unstructured Transmission-Line Modelling and Optimal Delaunay Triangular Meshes

Kaiqi Yan, Ana Vukovic, Phillip Sewell, and Trevor M. Benson

***Abstract*—The transmission-line modelling (TLM) method has been widely applied to many areas including electromagnetic and heat conduction problems. Its unstructured version, unstructured TLM (UTLM), however, has not hitherto been fully exploited in thermal diffusion problems. This paper derives in detail a thermal UTLM scheme to solve the two-dimensional diffusion equation numerically based on the optimal Delaunay triangular (ODT) mesh.**

***Index Terms*—simulation, diffusion equation, unstructured transmission-line modelling, optimal Delaunay triangulation**

I. Introduction

THE simulation of heat conduction is widely used in many areas of scientific research from electronics to medical applications. The heating happens as a result of another process such as microwave signal or lightning, and in order to fully describe the coupled electromagnetic (EM) and thermal phenomena, time-domain numerical methods are needed. An adequate choice of methodology within which to develop the multiphysics coupling is therefore important in terms of both numerical stability and computational efficiency. The algorithms to solve the thermal diffusion equation numerically in the time domain include the finite difference method [1], the finite volume method [2, 3] and the transmission-line modelling (TLM) method [4, 5]. Fully explicit finite difference schemes suffer from late time instability issues that are typical for large-scale problems. The stability condition can be improved using implicit schemes such as the Crank–Nicolson method, but they require matrix-solving which can become costly if the number of samples is large, especially when the algorithm is applied in higher dimensions [1]. One of the main advantages of the TLM method is its unconditional stability [6]. As an explicit scheme, the TLM method is also easy to parallelise and is therefore computationally efficient for large-scale problems.

The TLM method, originally developed for microwave applications, has been developed to solve diffusion equations via modelling the diffusion process as low-frequency waves in highly lossy media [4, 5]. Over the years, it has been applied to a variety of thermal diffusion problems such as the modelling of the heat conduction in transistors [7, 8], microwave food heating [9, 10], biomedical applications [11, 12] and nanoplasmonic heating [13]. Most of the reported methods use a structured grid for problem space discretisation. As the problem space becomes complex, unstructured (e.g. triangular or tetrahedral) meshes are preferred to describe the geometry because of their capability to reduce staircase effects at curved material interfaces and boundaries.

The application of the thermal unstructured TLM method on the bio-heat thermal diffusion modelling has been reported in [12], where the bio-energy equation was solved numerically; however, a non-Delaunay finite element mesh (Gmsh [14]) was used for space discretisation, which leads to two consequences: (a) The mesh is not optimally Delaunay and is prone to sliver triangles that typically cause numerical instabilities, and (b) the link lines in the formulation along which the heat flux propagates are not perpendicular to triangle edges. This discrepancy is assumed to be small, but then small and regular-shaped triangles are generally required, which is a limitation that affects not only the stability but also nonphysical dissipation, memory usage and accuracy (reported errors greater than 0.5% when compared against the analytical solution [12]).

The main goal of this paper is to develop the two-dimensional (2D) thermal version of the unstructured TLM method based on an optimal Delaunay triangular (ODT) mesh. The Delaunay mesh maximises the minimum angle among all triangles in the mesh and thus avoids the sliver triangles that typically occur in any practical mesh and cause numerical instabilities [15]. The optimal Delaunay triangulation (ODT) algorithm is applied after the initial Delaunay mesh generation to optimise the minimum link-line length.

Our paper is built on the concept of the EM unstructured TLM (UTLM) method using the 2D Delaunay mesh [16]. In the UTLM, the node centre is set to be the circumcentre of the triangle so that the link lines are perpendicular to the triangle edge. The time-stepping process models the scattering and connection of pulses at node centres and ports. The recommended time step is related to the minimum link line length in the mesh, which in many practical situations can be close to zero. In order to increase the simulation time step, a standard approach in the UTLM is to coalesce small cells with link-line lengths below a specified clustering threshold into a large cell in which scatterings and connections are solved implicitly, and it is applied after the ODT. This approach can increase the time step by one order of magnitude [16, 17].

The paper is organised as follows. Section II derives and maps the 2D thermal diffusion parameters to the transmission-line parameters for the case of the Delaunay triangular mesh. The connection and scattering process at triangle nodes and

Manuscript received Month Day, Year; revised Month Day, Year.

The authors are with the George Green Institute for Electromagnetics Research, University of Nottingham, Nottingham NG7 2RD, U.K.

ports are also introduced. Section III investigates the convergence and the accuracy of this thermal 2D UTLM method. A canonical test of the heat flow in a 2D square domain is conducted, and the accuracy is compared against the explicit Cartesian five-point finite difference scheme. Finally, the thermal UTLM is applied to characterise the temperature distribution on a power transistor with a heat sink.

II. Theory

A. Heat Diffusion Equation

We consider only the heat conduction here. If a substance is calorifically ideal, then its total heat energy Q can be expressed as

$$Q = c_p \rho_m T, \tag{1}$$

where ρ_m is the mass density, and c_p is the specific heat capacity at constant pressure.

By Fourier's law of thermal conduction in an isotropic medium, the heat flux $\boldsymbol{F}$ is calculated as

$$\boldsymbol{F} = -k_{th} \nabla T, \tag{2}$$

where k_{th} is the thermal conductivity.

The conservation of the total heat energy gives

$$\frac{\partial Q}{\partial t} + \nabla \cdot \boldsymbol{F} = Q_{VS}, \tag{3}$$

where Q_{VS} is the volume heat source.

Substituting (1) and (2) into (3) yields the thermal diffusion equation (4).

$$\frac{\partial T}{\partial t} = \frac{k_{th}}{c_p \rho_m} \nabla^2 T + \frac{Q_{VS}}{c_p \rho_m} \tag{4}$$

B. Derivation of Electric Component Quantities

In this section, we map the diffusion parameters onto the electric circuit parameters using the two-dimensional Delaunay [15] triangular mesh. Circumcentres of the Delaunay triangles are chosen as computational node centres, and adjacent node centres are connected by Voronoi [18] edges. The Voronoi mesh edges become the transmission-line network along which signals propagate. Fig. 1 shows two triangles with vertices A, B, C and D. The node centres P and Q are connected by the Voronoi mesh which also connects them to other neighbouring nodes. Point N represents the port connecting these two node centres and is positioned at the midpoint between P and Q. X and Y are the midpoints of PN and QN respectively, and they are used later in the midpoint rule approximation. The length of both PN and QN are guaranteed to be positive by the Delaunay mesh.

In the thermal TLM convention [4], the temperature is analogous to the voltage (5).

$$V \leftrightarrow T \tag{5}$$

The total two-dimensional heat flowing out of the quadrilateral $AXCY$ from $\overline{AXC}$ (denoted as left boundaries in this context) and $\overline{AYC}$ (denoted as right boundaries) are mapped to the analogous current I_L and I_R respectively, which are defined as (6) and (7), where $\widehat{\boldsymbol{n_0}}$ is the normal vector of the edge AC facing towards P (without loss of generality), and $\Delta l = |\overrightarrow{AC}|$. $\boldsymbol{G_L}$ and $\boldsymbol{G_R}$ are the equivalent uniform temperature gradients to give the same two-dimensional heat flowing out of two boundaries respectively, and this is to cope with the integral forms of the heat diffusion equations. Note that the subscripts $_L$ and $_R$ denote the left side (triangle ABC) and the right side (triangle ACD) respectively.

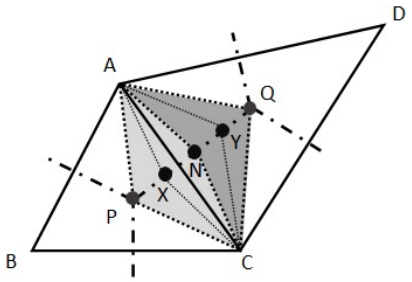

Fig. 1. Triangle ABC and triangle ADC are Delaunay triangles. P and Q are circumcentres as computational node centres. N is the port connecting two adjacent nodes. Dot-dashed lines are Voronoi edges. X and Y are the **midpoints** of PN and QN respectively.

$$\begin{aligned} I_L \leftrightarrow & \int_C^X (\boldsymbol{F} \cdot \hat{\boldsymbol{n}})\, dl + \int_X^A (\boldsymbol{F} \cdot \hat{\boldsymbol{n}})\, dl \\ & = -k_{th,L} \left(\boldsymbol{G_L} \cdot \widehat{\boldsymbol{n_0}}\right) \Delta l \end{aligned} \tag{6}$$

$$\begin{aligned} I_R \leftrightarrow & \int_A^Y (\boldsymbol{F} \cdot \hat{\boldsymbol{n}})\, dl + \int_Y^C (\boldsymbol{F} \cdot \hat{\boldsymbol{n}})\, dl \\ & = -k_{th,R} \left(\boldsymbol{G_R} \cdot -\widehat{\boldsymbol{n_0}}\right) \Delta l \end{aligned} \tag{7}$$

The integral forms of (2) and (3) are presented as (8) and (9) respectively.

$$\int_a^b \boldsymbol{F} \cdot d\boldsymbol{l} = -k_{th} \int_a^b \nabla T \cdot d\boldsymbol{l} = -k_{th} \left[T\right]_a^b \tag{8}$$

$$\frac{d}{dt} \iiint_V Q \cdot dV + \oiint_{\partial V} \boldsymbol{F} \cdot d\boldsymbol{A} = \iiint_V Q_{VS}\, dV \tag{9}$$

We choose the midpoint of PQ as the position of the port, and we firstly apply (8) from point N to point P. $\boldsymbol{G_L}$ is used to approximate the average temperature gradient along $\overrightarrow{NP}$.

$$\begin{aligned} \int_N^P \boldsymbol{F} \cdot d\boldsymbol{l} & \approx -k_{th,L} \left(\boldsymbol{G_L} \cdot \widehat{\boldsymbol{n_0}}\right) |\overrightarrow{NP}| \\ & = -k_{th,L} \left(T_P - T_N\right) \end{aligned} \tag{10}$$

Substituting (6) and (5) into (10) yields (11).

$$I_L \frac{|\overrightarrow{NP}|}{k_{th,L} \Delta l} = -\left(V_P - V_N\right) \tag{11}$$

According to $IR = -\Delta V$, the analogous resistance R_L is expressed as (12), where $\Delta_L = |\overrightarrow{NP}|$. Similarly, we apply (8) from point N to point Q to get the analogous resistance R_R, where $\Delta_R = |\overrightarrow{NQ}|$.

$$R_L = \frac{\Delta_L}{k_{th,L} \Delta l} \tag{12}$$

$$R_R = \frac{\Delta_R}{k_{th,R} \Delta l} \tag{13}$$

Applying (9) to the volume with the cross-section $AXCY$

gives (14), where Δz represents the fictitious unit length perpendicular to the paper plane.

$$\begin{aligned}\frac{d}{dt}&\left(\left(Q_L\frac{|\overrightarrow{XN}|}{2}+Q_R\frac{|\overrightarrow{YN}|}{2}\right)\Delta l\Delta z\right)\\&+\left(\oint_{AXCY}(\boldsymbol{F}\cdot\widehat{\boldsymbol{n}})\,dl\right)\Delta z\\&=\left(Q_{VS,L}\frac{|\overrightarrow{XN}|}{2}\Delta l+Q_{VS,R}\frac{|\overrightarrow{YN}|}{2}\right)\Delta z\end{aligned}\tag{14}$$

The area is calculated according to the fact that as a segment connecting two circumcentres, PQ perpendicularly bisects AC. Note that although the temperature T_N at the port N is not the same as the weighted average temperature of the quadrilateral $AXCY$, it is an adequate first-order approximation.

Substituting (5), (6), (7) and (1) into (14) yields (15).

$$\begin{aligned}I_L+I_R=&-\left(c_{p,L}\ \rho_{m,L}\frac{|\overrightarrow{XN}|}{2}\Delta l\right)\frac{dV_N}{dt}\\&-\left(c_{p,R}\ \rho_{m,R}\frac{|\overrightarrow{YN}|}{2}\Delta l\right)\frac{dV_N}{dt}\\&+Q_{VS,L}\frac{|\overrightarrow{XN}|}{2}\Delta l+Q_{VS,R}\frac{|\overrightarrow{YN}|}{2}\Delta l\end{aligned}\tag{15}$$

Note that I_L flows towards node centre P, and I_R flows towards node centre Q. According to $\Delta I=-C\cdot dV/dt+I_s$, the analogous capacitance C and the analogous current source I_s are expressed as (16) and (17) if the heat flowing into the two-dimensional domain due to the heat source is mapped to the current source.

$$C_{tot}=\frac{c_{p,L}\ \rho_{m,L}|\overrightarrow{XN}|\Delta l}{2}+\frac{c_{p,R}\ \rho_{m,R}|\overrightarrow{YN}|\Delta l}{2}\tag{16}$$

$$I_{s,tot}=Q_{VS,L}\frac{|\overrightarrow{XN}|}{2}\Delta l+Q_{VS,R}\frac{|\overrightarrow{YN}|}{2}\Delta l\tag{17}$$

To share the capacitance and the current source between two adjacent nodes, they are split intentionally.

$$C_L=\frac{c_{p,L}\ \rho_{m,L}\ \Delta_L\Delta l}{2}\tag{18}$$

$$C_R=\frac{c_{p,R}\ \rho_{m,R}\ \Delta_R\Delta l}{2}\tag{19}$$

$$I_{s,L}=\frac{Q_{VS,L}\ \Delta_L\Delta l}{2}\tag{20}$$

$$I_{s,R}=\frac{Q_{VS,R}\ \Delta_R\Delta l}{2}\tag{21}$$

The transmission-line circuit for the triangular cell ABC, as is used in Fig. 1, is shown in Fig. 2. The port voltages are denoted as V_i, and other transmission-line parameters, namely R_i, C_i and $I_{s,i}$ ($i=0,1,2$ denotes the edge (port) index) are obtained according to (12), (13), (18), (19), (20) and (21).

C. Transmission-Line Model

One UTLM node is connected to its neighbouring nodes via ports. The equivalent circuit at the port is illustrated in Fig. 3a, where R_L, R_R represent the resistance of the transmission-lines connecting two adjacent nodes, and C_L, C_R represent the capacitance of each transmission-line. The series link lines are used to replace capacitors in the thermal UTLM equivalent circuit. The characteristic impedance [4] of the capacitive series link lines is given as

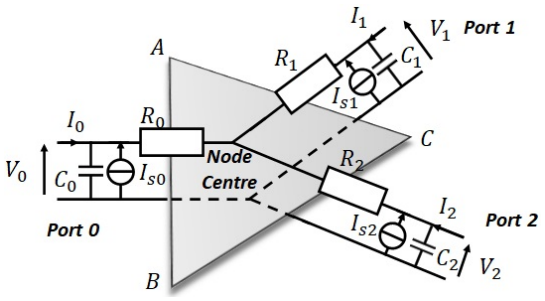

Fig. 2. Transmission-line Circuit of an Arbitrary Triangular Thermal UTLM Node (Triangle ABC is the computational cell)

$$Z_C=\frac{\Delta t}{C},\tag{22}$$

and the introduced error is in the associated error inductance of this link line which is expressed as

$$L_e=\frac{(\Delta t)^2}{C},\tag{23}$$

where Δt is the simulation time step.

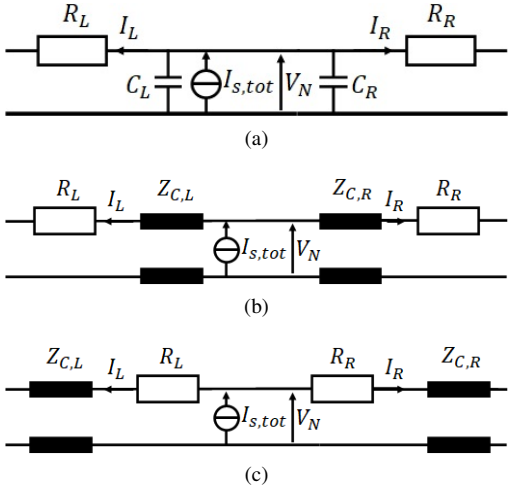

Fig. 3. (a) Transmission-line Circuit at a Port (b) Classic Resistor-Link Model (c) Alternative Link-Resistor Model

The transmission-line circuit (Fig. 3a) is turned into its resistor-link model shown in Fig. 3b, where the shunt capacitors are replaced by capacitive link lines with impedance given in (22). The position of the capacitive link line and its adjacent resistor in series could be exchanged, giving an alternative link-resistor model shown in Fig. 3c which is one of the optional ways to prevent the simulation data from excessively oscillating (known as the jump-to-zero problem [19]).

The thermal UTLM is unconditionally stable for all positive time step Δt because all electric component quantities are positive and hence physical. One only needs to consider

whether the wave behaviour is much less significant than the diffusion behaviour [4], which means that the inductive reactance ωL due to the error inductance (23) should be much less than the resistance in series (12) (13). Substituting the capacitance (18) (19) into this relationship yields

$$\omega \left(\Delta t\right)^2 \ll \min_{\text{all triangles}} \left\{ \frac{\Delta_i^2 c_p \rho_m}{2k_{th}} \right\}, \tag{24}$$

where ω is the frequency component of the solution, Δ_i the distance between a node centre and its port, and the subscript $_i$ denotes the edge index within a triangle.

After the equivalent circuit has been set up, scatterings and connections are executed alternately following the same principle as the regular TLM [4] algorithm. The Thévenin equivalent circuits used in the scattering computation at ports and node centres are demonstrated in Fig. 4a and Fig. 4b respectively, where V_N represents the middle voltage at the port, and V_M represents the middle voltage at the node centre.

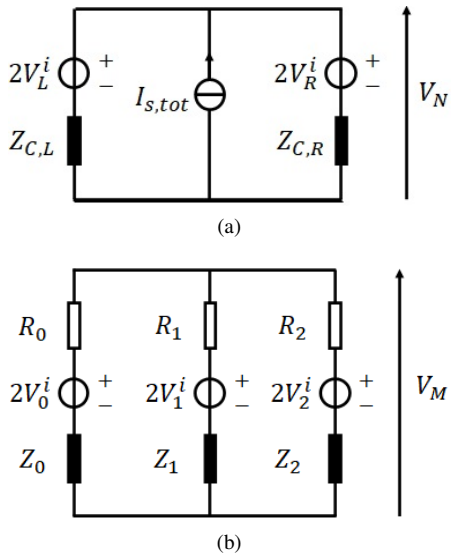

Fig. 4. Thévenin equivalent circuits used in the scattering and connection process (a) at ports (b) at node centres

By applying nodal voltage analysis to the equivalent circuit shown in Fig. 4a, the middle voltage V_N at the port is calculated as

$$V_N = \frac{I_{s,tot} + \frac{2V_L^i}{Z_{C,L}} + \frac{2V_R^i}{Z_{C,R}}}{\frac{1}{Z_{C,L}} + \frac{1}{Z_{C,R}}}. \tag{25}$$

Then, the reflected voltages are obtained by

$$V_L^r = V_N - V_L^i \tag{26}$$

$$V_R^r = V_N - V_R^i \tag{27}$$

In terms of the node centres, applying nodal voltage analysis to the circuit in Fig. 4b gives the middle voltage

$$V_M = \frac{\frac{2V_0^i}{R_0+Z_0} + \frac{2V_1^i}{R_1+Z_1} + \frac{2V_2^i}{R_2+Z_2}}{\frac{1}{R_0+Z_0} + \frac{1}{R_1+Z_1} + \frac{1}{R_2+Z_2}}. \tag{28}$$

The reflected voltages are obtained by

$$V_0^r = \left(V_M - \frac{V_M - 2V_0^i}{R_0 + Z_0} R_0 \right) - V_0^i, \tag{29}$$

$$V_1^r = \left(V_M - \frac{V_M - 2V_1^i}{R_1 + Z_1} R_1 \right) - V_1^i, \tag{30}$$

$$V_2^r = \left(V_M - \frac{V_M - 2V_2^i}{R_2 + Z_2} R_2 \right) - V_2^i. \tag{31}$$

The connection process is simply that the reflected voltages from the ports become the incident voltages towards their adjacent node centres, and the reflected voltages from the node centres become the incident voltages towards their ports.

D. Initial Conditions and Boundary Conditions

The initial temperature can be set up by specifying the incident voltages towards either the node centres or the ports before the scattering process of the first iteration. If the incident voltages towards the ports are initialised, then the scattering at the ports should be completed before the scattering at node centres in each iteration; on the other hand, if the incident voltages towards the node centres are initialised, then the scattering at the node centres should be done first instead. The initial incident voltage equals half of the initial temperature at the node centre in terms of quantity because the Thévenin equivalent circuit of the transmission-line has a voltage source of twice the incident voltage. If the classic resistor-link model (Fig. 3b) is used, we suggest that the incident voltages towards the node centre should be initialised to reduce small oscillations of the temperature during the simulation.

The boundary temperature is controlled by specifying the middle voltages at boundary ports during their scattering processes. This voltage equals the boundary temperature itself in terms of quantity and does not need to be halved.

E. Node Clustering and Mesh Optimisation

The suggested time step of the UTLM method is defined by the minimum link-line length in the mesh, i.e. PN length and QN length in Fig. 1. These lengths are always positive because P and N never cross over each other. This feature is guaranteed by the Delaunay mesh and is important for the stability of the UTLM method. In the situation where a link line length is very small or even zero, the cell resistance will be exceedingly large and the suitable simulation time step will be prohibitively small. To alleviate this problem, two adjacent nodes that share a very short link line need to be combined into a single quadrilateral node [16], which is illustrated in Fig. 5.

A capacitive stub is used to replace the short capacitive link lines. The characteristic impedance of the capacitive stub and its associated error inductance [4] are given as

$$Z_C = \frac{\Delta t}{2C}, \tag{32}$$

$$L_e = \frac{\left(\Delta t\right)^2}{4C}. \tag{33}$$

In a general Delaunay mesh, chances are that more than two triangular nodes should be combined together due to

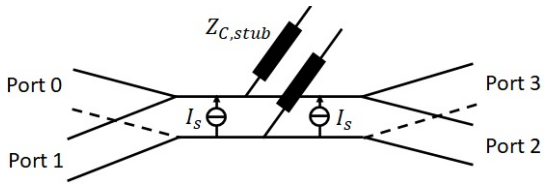

Fig. 5. Quadrilateral Clustered Node

small link line lengths in a similar manner, and this will add huge complexity to the code implementation. To mitigate this problem, we prefer to use the optimal Delaunay triangulation (ODT) mesh [20] [21] in practice which not only averages the shape of triangles and minimises the interpolation error but also maximises the minimum link line length [22]. When ODT is in place, only quadrilateral nodes and normal triangular nodes need to be considered as ODT eliminates the need for higher-level clustering. The ODT algorithm is available in detail in [21, 22].

Fig. 6 compares the Delaunay mesh of a 2D heat sink model before and after the ODT iterations. Please note that the structure is not coordinate-aligned along the y-axis and that in both cases the Delaunay triangulation provides smooth boundaries. These two histograms illustrate that the ODT mesh (Fig. 6b) leads to more uniform link-line lengths compared with the unoptimised mesh (Fig. 6a). The ratio between the maximum link line length and the minimum link line length can also be used as a measure of mesh uniformity, and it has reduced from 4173.1 to 151.7. Furthermore, the ODT mesh uses a smaller number of triangles (851) compared with the normal Delaunay mesh (876).

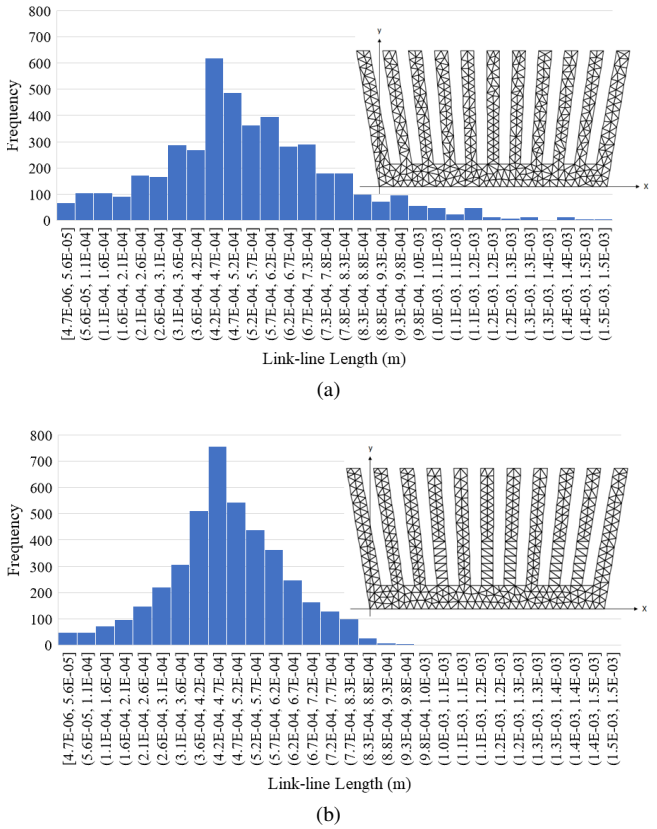

Fig. 6. (a) Normal Delaunay Triangular Mesh (876 Triangles) (b) ODT Mesh (851 Triangles). Histograms show the distributions of resultant link-line lengths. Insets are the meshes.

III. Results

A. Convergence Test using Unstructured Triangular Mesh

In this section, we evaluate the accuracy and convergence of the thermal unstructured TLM method by comparing its results against a known analytical solution. A canonical test is carried out first within a square computational domain $[-1, 1]$ (m) $\times$ $[-1, 1]$ (m). The physical parameters are specified as $\rho_m = 1.225$ kg $\cdot$ m^{-3}, $k_{th} = 0.0262$ W $\cdot$ m^{-1} $\cdot$ K^{-1} and $c_p = 1.005 \times 10^3$ J $\cdot$ kg^{-1} $\cdot$ K^{-1}. No heat source is placed in the domain. The initial temperature profile is set to $T(x, y, 0) = 298.15 + 75\cos\left(\frac{\pi}{2}x\right)\cos\left(\frac{\pi}{2}y\right)$, and the boundary temperature is fixed at 298.15 K. This test problem has an analytical solution given as $T(x, y, t) = 298.15 + 75\cos\left(\frac{\pi}{2}x\right)\cos\left(\frac{\pi}{2}y\right)\exp\left(-\alpha\frac{\pi^2}{2}t\right)$, where $\alpha = k_{th}/(\rho_m c_p)$.

The square computational domain is triangulated using different numbers of elements, and the ODT mesh optimisation is applied before the simulation. A constant time step of $\Delta t = 2 \times 10^{-1}$ s is used in this convergence test, and the stop time t_{stop} is set to 5×10^4 s. The thermal UTLM algorithm runs with ODT meshes of different numbers of elements respectively. The temperature at every UTLM node centre is recorded and compared with the analytical solution, and the RMS Error $= \sqrt{(\sum_{i=1}^{N} e_i^2)/N}$ is used as the criterion to assess the overall error, where e_i is the absolute error of temperature at each node centre, and N is the number of nodes. The RMS error obtained from each mesh is plotted in Fig. 7, and as is shown, it decreases as the mesh becomes finer, i.e. as the number of triangles in the mesh increases.

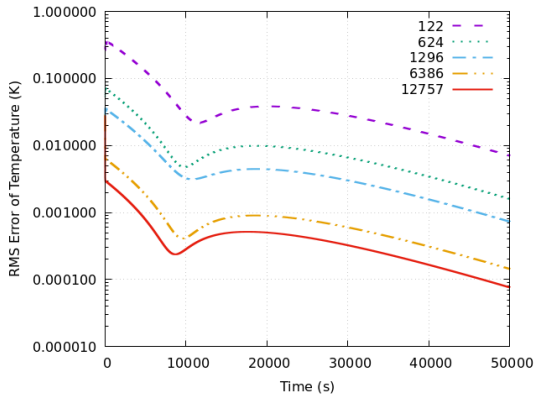

Fig. 7. RMS error of temperature obtained using different number of triangles.

Fig. 8 shows the computational domain of the problem with 122 and 1296 cells and the corresponding temperature distribution at $t_{stop} = 5 \times 10^4$ s for these two meshes. It is seen that the finer mesh provides much smoother field profiles.

A further error analysis is shown in Fig. 9, where the RMS error at $t = 10^4$ s is plotted against the average distance between adjacent node centres (Δx) in logarithmic scale. Δx

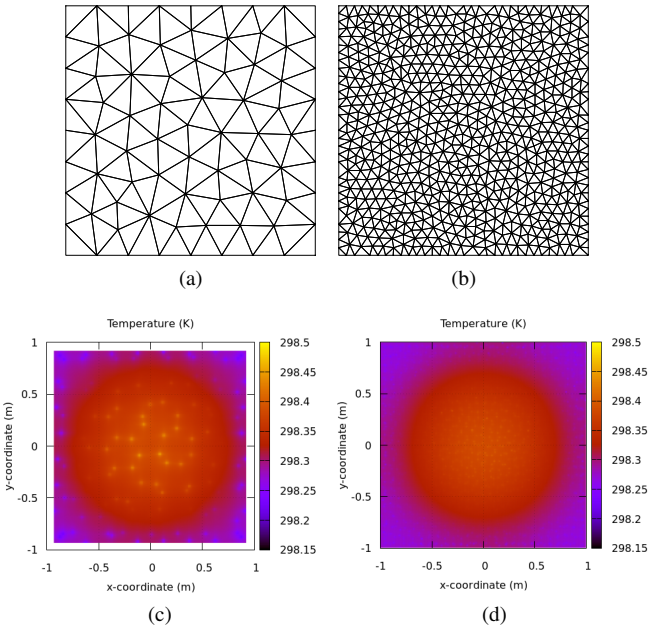

Fig. 8. ODT Meshes and Simulation Results (a) ODT Mesh (122 Triangles) (b) ODT Mesh (1296 Triangles) (c) Final Temperature (122 Triangles) (d) Final Temperature (1296 Triangles)

is approximated using the number of triangles and the total area of the computational domain, and it is equivalent to the average mesh element size. The gradient of the trendline in Fig. 9 confirms the second-order average local spatial accuracy of the thermal unstructured TLM (UTLM) method.

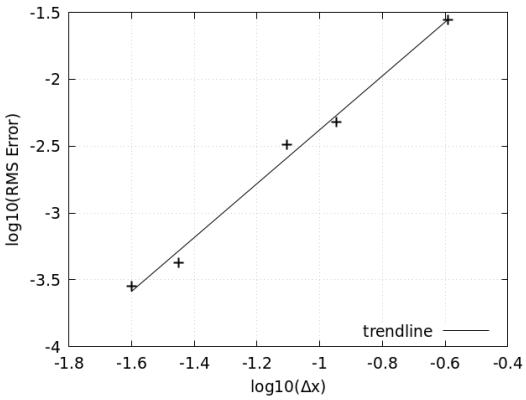

Fig. 9. RMS Error at $t = 10^4$ s of Different Mesh Resolutions in Logarithmic Scale

B. Mesh with Quadrilateral Combined Nodes

To test the quadrilateral combined node, structured meshes containing only right-angled triangles are deliberately created for the thermal UTLM algorithm. Every pair of right-angled triangles in a square unit become clustered, i.e. combined automatically into a quadrilateral node because their circumcentres coincide. The thermal UTLM results are compared against the fully explicit five-point finite difference scheme as

$$T_{i,j}^{n+1} = T_{i,j}^{n} + \alpha \frac{\Delta t}{\Delta x^2}(T_{i+1,j}^{n} + T_{i-1,j}^{n} + T_{i,j+1}^{n} + T_{i,j-1}^{n} - 4 \cdot T_{i,j}^{n}) \tag{34}$$

with a time step limit of $(\alpha \Delta t)/\Delta x^2 < 1/4$.

The finite difference algorithm runs with two different grid resolutions, namely 200×200 and 400×400 Cartesian nodes, and the thermal UTLM runs with a 100×100 square-structured mesh ($20,000$ right-angled triangles). The time step used in the finite difference method is 2×10^{-2} s (under the stability condition), and the time step used in the thermal UTLM is kept as $\Delta t = 2 \times 10^{-1}$ s. The same canonical test as in Fig. 7 is used, and Fig. 10 shows the RMS errors obtained from three simulations. Fig. 10 proves the correctness of the thermal UTLM method with quadrilateral combined nodes, and it also illustrates that the thermal UTLM method can achieve slightly better accuracy with a lower gird resolution and a larger time step compared with the fully explicit five-point finite difference scheme, although more memory is required for computation. The spike in Fig. 10 is due to the fact that the numerical results from the UTLM method oscillate around the exact solution, but as the simulation time increases the envelope of the error is smoothly decreasing.

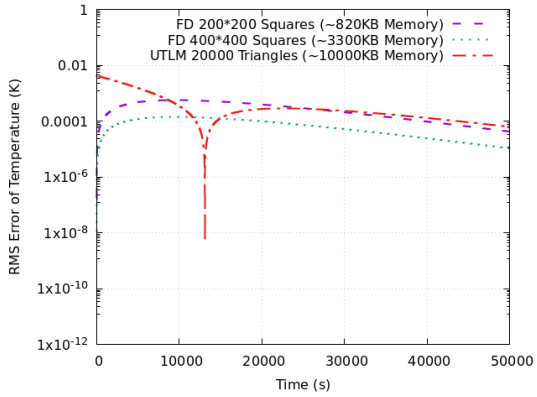

Fig. 10. RMS Error of Temperature obtained using the Fully Explicit Finite Difference Scheme and the Thermal UTLM Scheme

C. Simulation of Power Transistor

The thermal UTLM has the advantage of being able to simulate real engineering cases particularly when non-Cartesian boundaries and multiple materials are involved. This section demonstrates an example simulation of the temperature profile around a power transistor with a heat sink on top. The schematic of the physical model and the layout of the computational domain is shown in Fig. 11, where the power transistor is modelled as silicon, and the heat sink is modelled as copper. The physical parameters of silicon, copper and the surrounding air taken in this simulation are listed in Table I [8], and the volume heat source of the silicon region is specified as $Q_{VS} = 9 \times 10^5$ W $\cdot$ m^{-3} to describe a typical heat dissipation.

The initial temperature across the whole domain is set to 298.15 K, and the boundary temperature is fixed as 298.15 K.

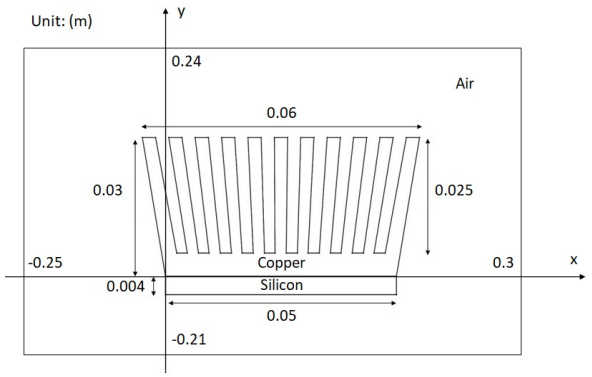

Fig. 11. Layout of a heat sink on top of a power transistor. The fins and the air gaps have the same width and evenly divide the top and bottom of the trapezoidal shape. The scale of the outer rectangular boundary is for illustration purposes only and does not match the scale of the axes.

TABLE I
PHYSICAL PARAMETERS SETUP

Material	k_{th} $(\mathrm{W}/(\mathrm{m}\cdot\mathrm{K}))$	ρ_m $(\mathrm{kg}/\mathrm{m}^3)$	c_p $(\mathrm{J}/(\mathrm{kg}\cdot\mathrm{K}))$
Air	0.0262	1.225	1005
Silicon	148	2320	700
Copper	393	8960	276

The temperature distribution after 5 s and 300 s is shown in Fig. 12a and Fig. 12b respectively. In this simulation, an ODT mesh with 978649 triangles generated by the ODT algorithm is used, and the time step is chosen as $\Delta t = 2 \times 10^{-2}$ s. It is seen that the thermal UTLM method based on the ODT mesh can keep being stable and produce a reasonable solution with smooth temperature transitions at all material interfaces, which indicates the great reliability of our proposed method particularly for unstructured complicated geometries and multi-material heat transfers.

Note that the diffusion equation only models heat conduction, so convection and radiation are not considered in this simulation. Although techniques such as using the equivalent thermal conductivity with the Nusselt number [23] can be applied, they are beyond the scope of this paper.

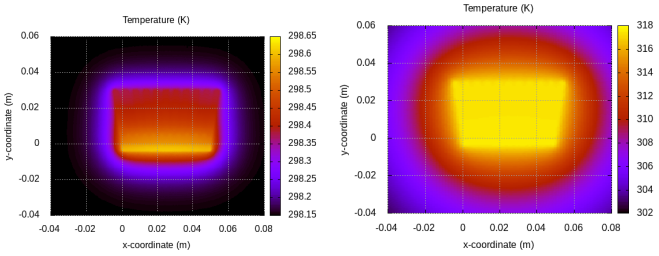

(a) (b)

Fig. 12. Temperature Distribution around the Transistor with a Heat Sink after (a) 5 s (b) 300 s.

IV. CONCLUSION

The two-dimensional UTLM method using the ODT mesh has been presented and applied to solve the thermal diffusion equation numerically. The heat diffusion equation is mapped onto the equivalent transmission-line parameters, and the spatial second-order average local accuracy of this scheme has been shown. This thermal UTLM method using the ODT mesh is shown to be correct, stable and reliable when the physical model involves complicated boundary shapes and multi-material profiles. Also, this time-domain thermal UTLM method is not limited by the CFL condition on the time step, and as an explicit scheme, it does not require matrix-solving either, which is the main advantage against both implicit schemes and other explicit schemes. This makes it ideally suitable for the modelling of coupled electrothermal problems.

ACKNOWLEDGMENT

This work was supported by the Faculty of Engineering Research Excellence PhD Scholarship, University of Nottingham.

REFERENCES

[1] A. Faul, *A Concise Introduction to Numerical Analysis*. Taylor & Francis Inc, Mar 2016.

[2] J. Breil and P.-H. Maire, "A cell-centered diffusion scheme on two-dimensional unstructured meshes," *Journal of Computational Physics*, vol. 224, pp. 785–823, 2006.

[3] P.-H. Maire and J. Breil, "A high-order finite volume cell-centered scheme for anisotropic diffusion on two-dimensional unstructured grids," *Journal of Computational Physics*, vol. 11, pp. 76–15, 2011.

[4] C. Christopoulos, *The Transmission-Line Modeling Method: TLM*. Wiley-IEEE Press, 1995.

[5] D. de Cogan, "Propagation analysis for thermal modeling," *IEEE Transactions on Components, Packaging, and Manufacturing Technology: Part A*, vol. 21, no. 3, pp. 418–423, 1998.

[6] P. B. Johns, "A simple explicit and unconditionally stable numerical routine for the solution of the diffusion equation," *International Journal for Numerical Methods in Engineering*, vol. 11, no. 8, pp. 1307–1328, 1977.

[7] P. W. Webb and I. A. D. Russell, "Application of the TLM method to transient thermal simulation of microwave power transistors," *IEEE Transactions on Electron Devices*, vol. 42, no. 4, pp. 624–631, 1995.

[8] R. Hocine, M. A. Boudghene Stambouli, and A. Saidane, "A three-dimensional TLM simulation method for thermal effect in high power insulated gate bipolar transistors," in *Eighteenth Annual IEEE Semiconductor Thermal Measurement and Management Symposium. Proceedings 2002 (Cat.No.02CH37311)*, pp. 99–104, 2002.

[9] C. Flockhart, V. Trenkic, and C. Christopoulos, "The simulation of coupled electromagnetic and thermal problems in microwave heating," in *1994 Second International Conference on Computation in Electromagnetics*, pp. 267–270, 1994.

[10] C. Christopoulos, "The application of time-domain numerical simulation methods to the microwave heating of foods," *IMA Journal of Management Mathematics*, vol. 5, pp. 385–397, Jan 1993.

[11] A. Amri, A. Saidane, and S. Pulko, "Thermal analysis of a three-dimensional breast model with embedded tumour using the transmission line matrix (tlm) method," *Computers in Biology and Medicine*, vol. 41, no. 2, pp. 76–86, 2011.
[12] H. Milan and K. Gebremedhin, "Triangular node for transmission-line modeling (TLM) applied to bio-heat transfer," *Journal of Thermal Biology*, vol. 62, pp. 116–122, 2016.
[13] A. Elkalsh, P. Sewell, T. M. Benson, and A. Vukovic, "Coupled electrothermal two-dimensional model for lightning strike prediction and thermal modeling using the TLM method," *IEEE Journal on Multiscale and Multiphysics Computational Techniques*, vol. 2, pp. 38–48, 2017.
[14] C. Geuzaine and J.-F. Remacle, "Gmsh: A three-dimensional finite element mesh generator with built-in pre-and post-processing facilities," *International Journal for Numerical Methods in Engineering*, vol. 79, pp. 1309–1331, 2009.
[15] J. R. Shewchuk, "Triangle: A two-dimensional quality mesh generator and delaunay triangulator." https://www.cs.cmu.edu/~quake/triangle.html.
[16] P. Sewell, J. G. Wykes, T. M. Benson, C. Christopoulos, D. W. P. Thomas, and A. Vukovic, "Transmission-line modeling using unstructured triangular meshes," *IEEE Transactions on Microwave Theory and Techniques*, vol. 52, no. 5, pp. 1490–1497, 2004.
[17] P. Sewell, T. M. Benson, C. Christopoulos, D. W. P. Thomas, A. Vukovic, and J. G. Wykes, "Transmission-line modeling (TLM) based upon unstructured tetrahedral meshes," *IEEE Transactions on Microwave Theory and Techniques*, vol. 53, no. 6, pp. 1919–1928, 2005.
[18] E. Tonti, "Finite formulation of electromagnetic field," *IEEE Transactions on Magnetics*, vol. 38, no. 2, pp. 333–336, 2002.
[19] D. de Cogan, "Time-step changes and parity effects in TLM thermal models," in *International Conference on Simulation '98. (Conf. Publ. No. 457)*, pp. 325–328, 1998.
[20] L. Chen and J. Xu, "Optimal delaunay triangulations," *Journal of Computational Mathematics*, vol. 22, no. 2, pp. 299–308, 2004.
[21] P. Alliez, D. Cohen-Steiner, M. Yvinec, and M. Desbrun, "Variational tetrahedral meshing," *ACM SIGGRAPH 2005*, pp. 617–625, 2005.
[22] S. Cole, P. Sewell, A. Vukovic, and T. M. Benson, "Adaptive meshing for optical resonators," in *2012 14th International Conference on Transparent Optical Networks (ICTON)*, pp. 1–4, 2012.
[23] Y. Spaeck-Leigsnering, M. Koch, C. Bergfried, E. Gjonaj, H. De Gersem, and M. Heckel, "Electrothermal finite element analysis of a pluggable high voltage surge arrester," in *VDE High Voltage Technology 2020; ETG-Symposium*, pp. 1–7, 2020.

Kaiqi Yan received a First Class BEng (Hons) degree in Electrical and Electronic Engineering and the IET Prize at the University of Nottingham in 2018, and a Distinction MPhil degree in Scientific Computing and the Jennings Prize at Wolfson College, the University of Cambridge in 2019. He is currently working towards a PhD degree in Electrical and Electronic Engineering at the University of Nottingham supported by the Faculty of Engineering Research Excellence PhD Scholarship. His research interests include but are not limited to the numerical and geometrical modelling of physical phenomena and engineering applications via developing computational fluid dynamics (CFD) and computational electromagnetics (CEM) codes in C++.

Ana Vukovic was born in Nis, Serbia, in 1968. She received the Diploma of Engineering degree in electronics and telecommunications from the University of Nis, Nis, Yugoslavia, in 1992, and the Ph.D. degree from the University of Nottingham, Nottingham, U.K., in 2000. From 1992 to 2001, she was a Research Associate with the University of Nottingham. In 2001, she joined the School of Electrical and Electronic Engineering, University of Nottingham, as a Lecturer. In 2008 and 2020, she became an Associate Professor and Professor of Electromagnetic Applications at the University of Nottingham.Her research interests are electromagnetics with a particular emphasis on applications in optoelectronics, microwaves, EMC and aerospace.

Phillip Sewell was born in London, U.K., in 1965. He received the B.Sc. degree in electrical and electronic engineering (with first-class honors) and Ph.D. degree from the University of Bath, Bath, U.K., in 1988 and 1991, respectively. From 1991 to 1993, he was a Post-Doctoral Fellow with the University of Ancona, Ancona, Italy. In 1993, he became a Lecturer with the School of Electrical and Electronic Engineering, University of Nottingham, Nottingham, U.K. In 2001 and 2005, he became a Reader and Professor of electromagnetics at the University of Nottingham. His research interests involve analytical and numerical modeling of electromagnetic problems with application to opto-electronics, microwaves and aerospace applications.

Trevor M. Benson received a First Class honors degree in Physics and the Clark Prize in Experimental Physics from the University of Sheffield in 1979, a PhD in Electronic and Electrical Engineering from the same University in 1982, and the DSc degree from the University of Nottingham in 2005. After spending over six years as a Lecturer at University College Cardiff, Professor Benson moved to The University of Nottingham in 1989. He was promoted to a Chair in Optoelectronics in 1996, having previously been Senior Lecturer (1989) and Reader (1994). Since August 2020 he is Professor Emeritus. Professor Benson's research interests include experimental and numerical studies of electromagnetic fields and waves with particular emphasis on the theory, modeling and simulation of optical waveguides, lasers and amplifiers, nanoscale photonic circuits and electromagnetic compatibility. He is a Fellow of the Royal Academy of Engineering (FREng), the Institute of Engineering Technology (FIET), the European Optical Society (FEOS) and the Institute of Physics (FInst.P).